

A HIGHER EFFICIENCY OF CONVERTING GAS TO STARS PUSHES GALAXIES AT $z \sim 1.6$ WELL-ABOVE THE STAR-FORMING MAIN SEQUENCE

J. D. SILVERMAN¹, E. DADDI², G. RODIGHIERO³, W. RUJOPAKARN^{1,4}, M. SARGENT⁵, A. RENZINI⁶, D. LIU², C. FERUGLIO⁷, D. KASHINO⁸, D. SANDERS⁹, J. KARTALTEPE¹⁰, T. NAGAO¹¹, N. ARIMOTO¹², S. BERTA¹³, M. BÉTHÉMIN¹⁴, A. KOEKEMOER¹⁵, D. LUTZ¹³, G. MAGDIS^{16,17}, C. MANCINI⁶, M. ONODERA¹⁸, G. ZAMORANI¹⁹

Published in The Astrophysical Journal Letters

ABSTRACT

Local starbursts have a higher efficiency of converting gas into stars, as compared to typical star-forming galaxies at a given stellar mass, possibly indicative of different modes of star formation. With the peak epoch of galaxy formation occurring at $z > 1$, it remains to be established whether such an efficient mode of star formation is occurring at high-redshift. To address this issue, we measure the molecular gas content of seven high-redshift ($z \sim 1.6$) starburst galaxies with the Atacama Large (sub-)Millimeter Array and IRAM/Plateau de Bure Interferometer. Our targets are selected from the sample of Herschel far-infrared detected galaxies having star formation rates ($\sim 300\text{--}800\text{ M}_{\odot}\text{ yr}^{-1}$) elevated ($\gtrsim 4\times$) above the star-forming ‘main sequence’, and included in the FMOS-COSMOS near-infrared spectroscopic survey of star-forming galaxies at $z \sim 1.6$ with Subaru. We detect CO emission in all cases at high levels of significance, indicative of high gas fractions ($\sim 30\text{--}50\%$). Even more compelling, we firmly establish with a clean and systematic selection that starbursts, identified as main-sequence outliers, at high redshift generally have a lower ratio of CO to total infrared luminosity as compared to typical main-sequence star-forming galaxies, although with a smaller offset than expected based on past studies of local starbursts. We put forward a hypothesis that there exists a continuous increase in star formation efficiency with elevation from the main sequence with galaxy mergers as a possible physical driver. Along with a heightened star formation efficiency, our high-redshift sample is similar in other respects to local starbursts such as being metal rich and having a higher ionization state of the interstellar medium.

Subject headings: galaxies: ISM — galaxies: high-redshift — galaxies: starburst — galaxies: star formation

john.silverman@ipmu.jp

¹ Kavli Institute for the Physics and Mathematics of the Universe (WPI), The University of Tokyo Institutes for Advanced Study, The University of Tokyo, Kashiwa, Chiba 277-8583, Japan

² Laboratoire AIM, CEA/DSM-CNRS-Université Paris Diderot, Irfu/Service d’Astrophysique, CEA Saclay

³ Dipartimento di Fisica e Astronomia, Università di Padova, vicolo Osservatorio, 3, 35122, Padova, Italy

⁴ Department of Physics, Faculty of Science, Chulalongkorn University, 254 Phayathai Road, Pathumwan, Bangkok 10330, Thailand

⁵ Astronomy Centre, Department of Physics and Astronomy, University of Sussex, Brighton, BN1 9QH, UK

⁶ Istituto Nazionale de Astrofisica, Osservatorio Astronomico di Padova, v.co dell’Osservatorio 5, I-35122, Padova, Italy, EU

⁷ IRAM - Institut de RadioAstronomie Millimétrique, 300 rue de la Piscine, 38406 Saint Martin d’Hères, France

⁸ Division of Particle and Astrophysical Science, Graduate School of Science, Nagoya University, Nagoya, 464-8602, Japan

⁹ Institute for Astronomy, University of Hawaii, 2680 Woddlawn Drive, Honolulu, HI, 96822

¹⁰ National Optical Astronomy Observatory, 950 N. Cherry Ave., Tucson, AZ, 85719

¹¹ Graduate School of Science and Engineering, Ehime University, 2-5 Bunkyo-cho, Matsuyama 790-8577, Japan

¹² Subaru Telescope, 650 North A’ohoku Place, Hilo, Hawaii, 96720, USA

¹³ Max-Planck-Institut für extraterrestrische Physik, D-84571 Garching, Germany

¹⁴ European Southern Observatory, Karl-Schwarzschild-Str. 2, 85748 Garching, Germany

¹⁵ Space Telescope Science Institute, 3700 San Martin Drive, Baltimore, MD, 21218, USA

¹⁶ Department of Physics, University of Oxford, Keble Road, Oxford OX1 3RH, UK

¹⁷ Institute for Astronomy, Astrophysics, Space Applications and Remote Sensing, National Observatory of Athens, GR-15236 Athens, Greece

¹⁸ Institute of Astronomy, ETH Zürich, CH-8093, Zürich, Switzerland

¹⁹ INAF Osservatorio Astronomico di Bologna, via Ranzani 1, I-40127, Bologna, Italy

1. INTRODUCTION

It has recently come to light that the growth of galaxies may be less erratic than previously thought. The existence of a tight relation between the stellar mass (M_*) and star formation rate (SFR) of star-forming galaxies, termed the ‘main sequence’ (MS; Noeske et al. 2007; Daddi et al. 2007; Elbaz et al. 2007; Whitaker et al. 2012; Kashino et al. 2013; Speagle et al. 2014) is indicative of a quasi-equilibrium being maintained between gas supply, SFR, and gas expulsion from galaxies (e.g., Bouch   et al. 2010; Lilly et al. 2013). This SFR- M_* relation evolves strongly with look-back time, paralleling the global evolution of the cosmic SFR density from the present to $z \sim 2$ (Madau & Dickinson 2014). It is becoming clear that such a decline in SFR is in response to diminishing gas reservoirs (e.g., Tacconi et al. 2013; Scoville et al. 2014; Santini et al. 2014). The efficiency of star formation ($SFE \equiv SFR/M_{gas}$), i.e., the efficiency at which gas is being converted to stars, is remarkably similar across a wide range of cosmic time within the global star-forming population, usually with gas mass M_{gas} inferred from the CO molecular line luminosity L'_{CO} (e.g., Tacconi et al. 2010, 2013; Daddi et al. 2010b).

However, outliers from the MS are known to exist, with very high specific SFR (sSFR) compared to normal MS galaxies, such as local ultra-luminous infrared galaxies (ULIRG, Sanders & Mirabel 1996). At $z \sim 2$, these MS outliers represent $\sim 2\%$ of the star-forming population and contribute only a moderate fraction ($\sim 10\%$) of the global co-moving SFR-density (Rodighiero et al. 2011). Yet, they are still likely to play an important role in galaxy evolution, as a high fraction of galaxies may experience such a star-bursting event. Therefore, it is important to understand the physical conditions that can lead to such a surge in SFR.

Local starbursts have a higher SFE compared to MS galaxies. Estimates of their molecular gas content from their CO luminosity indicate that a given gas mass is capable of producing higher SFRs (Solomon et al. 1997), and a bi-modal distribution of SFEs has been proposed for the general MS and outlier population (Daddi et al. 2010b; Genzel et al. 2010). While there are uncertainties with respect to the appropriate conversion of L'_{CO} to H_2 gas mass (α_{CO}), an offset with respect to MS galaxies is already apparent when considering the observed quantities L'_{CO} and total infrared luminosity (L_{TIR}). The physical mechanism responsible for this enhanced SFE is not entirely clear and one cannot exclude that sample selection may be responsible for the lack of galaxies with intermediate SFEs. While CO detections have been obtained for high-redshift submm-selected galaxies (SMGs; e.g., Greve et al. 2005; Bothwell et al. 2013) and star-forming radio galaxies (SFRG; Casey et al. 2011), these samples do not cleanly distinguish starburst outliers from the MS population and submm selected samples could be biased towards galaxies with lower dust temperatures (Magnelli et al. 2014). Therefore, it is imperative to study the CO emission of starbursts securely elevated above the MS at their respective stellar mass and near the peak epoch of star formation ($z \sim 2$). Rodighiero et al. (2011) achieve such a clear distinction between MS and MS-outlier galaxies using large photo-

metric samples with multi-wavelength coverage, including the bulk of the FIR emission. Our targets then result in a homogenous sample that does not have contaminants such as those inherent with other selections.

To address this issue, we report on interferometric observations of the molecular transition ^{12}CO 2-1 and ^{12}CO 3-2 for a sample of seven MS outliers using both the Atacama Large Millimeter Array (ALMA) and IRAM Plateau de Bure Interferometer. Our sample is extracted from the 246 MS outliers (with sSFRs $\gtrsim 4\times$ above the mean of the MS; Figure 1) at $1.4 < z < 2.5$ identified with Herschel observations over the COSMOS field (Rodighiero et al. 2011) that effectively cover the peak FIR emission. Among these Herschel-detected galaxies, those with photometric redshifts between 1.4 and 1.7 are observed through our Subaru Intensive Project (Silverman et al. 2015) with the FMOS near-IR multi-object spectrograph. These spectra provide a detection of key diagnostic emission lines (i.e., $H\alpha$, $H\beta$, $[NII]\lambda 6585$, $[OIII]\lambda 5008$) used to measure accurate spectroscopic redshifts, SFRs, and metallicities. Six targets, labeled in Figure 1, are extracted from this sample with an additional galaxy at a slightly higher redshift (PACS-282; $z = 2.19$) where the redshift comes from the zCOSMOS-Deep program (Lilly et al. 2007).

Our confidence in these galaxies being ‘outliers’ in the SFR- M_* plane is based on the exquisite multi-wavelength coverage of the COSMOS field. Stellar masses are derived from SED-fitting using Hyperz with stellar population synthesis models (Bruzual & Charlot 2003) at the respective spectroscopic redshift. The deblending of detections in Herschel (or $70\mu m$ *Spitzer*) images relies upon *Spitzer* MIPS $24\mu m$ priors. SFRs are derived from L_{TIR} , an integral of the best-fit model SED (Draine & Li 2007) from 8 - 1000 μm using the *Spitzer* ($24\mu m$), Herschel PACS (100 and 160 μm) and SPIRE (250, 350 and 500 μm) bands, thus accounting for the obscured star formation as in Magdis et al. (2012). Moreover, four of the seven galaxies have 1.4 GHz radio detections at $> 5\sigma$ level (Schinnerer et al. 2010) and radio-based SFRs are consistent with being above the MS. The presence of strong AGN within our sample is ruled out by the lack of individual X-ray detections by *Chandra*. Even if an obscured AGN were present, the contribution to L_{TIR} would be negligible (Rodighiero et al. 2011; Pozzi et al. 2012). Throughout this work, we assume $H_0 = 70 \text{ km s}^{-1} \text{ Mpc}^{-1}$, $\Omega_\Lambda = 0.7$, $\Omega_M = 0.3$, and use a Salpeter IMF for SFRs and stellar masses.

2. OBSERVATIONS OF CO EMISSION AT HIGH-Z

ALMA observations of five galaxies were carried out in Cycle 1 (Project 2012.1.00952.S) using 25-30 12m antennas and the band 3 receiver tuned to intermediate frequencies between 86.395 - 94.888 GHz with a resolution of 488 kHz and spectral bandpass of 1.875 GHz. Two ‘scheduling blocks’ (SB1 and SB2) were defined to accommodate the requirements to detect CO 2-1 within a single sideband for each of our targets (SB1: PACS-819, 830; SB2: PACS-325, 299 and 867). On-source exposure times were 32 minutes (819 and 830), 2.3 hours (299 and 325) and 3.8 hours (867) that met our request based on predictions of CO emission from their IR luminosity and an assumed ratio L_{CO}/L_{TIR} ($3\times$ lower than MS galaxies). The antenna configurations had baselines

Table 1
Sample data and CO measurements^a

ID	RA (CO)	Dec (CO)	z_{CO} ^b	z_{spec} ^c	$\log M_*$ ^d M_\odot	SFR ^e	I_{CO} ^f Jy km s ⁻¹	L'_{CO} ^g	Δv ^h	CO size (")	Gas ⁱ fraction
299	09:59:41.31	02:14:42.91	1.6483	1.6467	10.44	554 \pm 40	0.67 \pm 0.08	10.44	590	<2.4	0.52
325	10:00:05.47	02:19:42.61		1.6557	10.29	139 \pm 10	0.28 \pm 0.06	10.07	764		0.32
819	09:59:55.55	02:15:11.70	1.4451	1.4449	10.61	783 \pm 18	1.10 \pm 0.07	10.55	592	0.34 \pm 0.08	0.34
830	10:00:08.75	02:19:01.90	1.4631	1.4610	10.86	517 \pm 12	1.18 \pm 0.10	10.59	436	0.97 \pm 0.17	0.46
867	09:59:38.12	02:28:56.56	1.5656	1.5673	10.67	358 \pm 34	0.46 \pm 0.04	10.24	472	<1.5	0.29
282	10:00:01.54	02:11:24.27	2.1869	2.1924	10.88	581 \pm 42	0.75 \pm 0.12	10.44	660	<3.4	0.28
164	10:01:30.53	01:54:12.96	1.6481	1.6489	>10.28	358 \pm 8	0.61 \pm 0.11	10.40	894	<4.8	0.52

^a The first five targets are observed with ALMA while the remaining two with PdBI.

^b $\sigma_z = 0.0003$ -0.0004. An accurate CO centroid was not obtained for 325 thus the H α redshift was used for the CO flux measurement.

^c Spectroscopic redshifts are based on H α with the exception of #282 and have errors $\sigma_{\Delta z/(1+z)} = 1.8 \times 10^{-4}$.

^d $\sigma_M \sim 0.07$ dex (Ilbert et al. 2015)

^e Units of $M_\odot \text{ yr}^{-1}$.

^f All are based on the CO 2-1 transition with the exception of 282 (3-2).

^g Log base 10; units of K km s⁻¹ pc²

^h Full width of the CO line at zero intensity in units of velocity (km s⁻¹).

ⁱ $f_{gas} = M_{gas}/(M_* + M_{gas})$

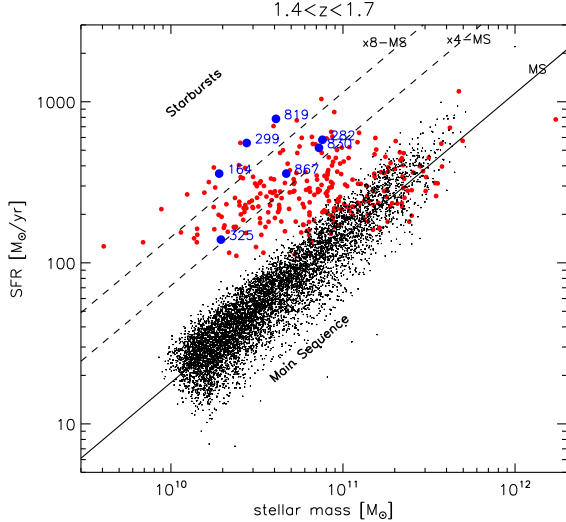


Figure 1. SFR versus M_* for galaxies with $1.4 < z < 1.7$ in COSMOS. Galaxies with CO observations are shown in blue. For reference, we plot star-forming galaxies that denote the MS (small dots). *Herschel*-detected galaxies include our sample in blue and those shown in red.

up to $\sim 400m$ ($\sim 200m$) for SB1 (SB2) thus resulting in a beam size (FWHM) of $1.3'' \times 1.0''$ ($4.5'' \times 2.0''$; $5.4'' \times 2.7''$ for PACS 325 only). The images of PACS-819 (830) have a flux sensitivity level of 0.12 (0.10) mJy beam⁻¹ over a bandwidth of 400 km s⁻¹ while the deeper observations reach 0.073 - 0.14 mJy beam⁻¹ for the same spectral window. Standard targets were used for flux (Mars, Ganymede), bandpass, and phase calibration.

We measure the CO flux by fitting the data in UV space with the GILDAS task ‘uvfit’ available in the MAPPING package. The fit was performed using a point source model or a circular Gaussian for resolved sources that returns the centroid, de-convolved source size, and integrated flux. We find good agreement between fluxes returned from GILDAS with those using ‘imfit’ in the image plane with CASA. Additionally, we resolve the emission for PACS- 819 and 830; therefore, a measure of the source extent is reported.

To increase the sample size, interferometric measure-

ments were obtained with IRAM/PdBI for PACS-282 (CO 3-2) and PACS-164 (CO 2-1). For PACS-282 (PACS-164), an integration time of 6.2 (12.9) hours, using the 3mm band in configuration D, was achieved that resulted in a limiting 1σ sensitivity level of 0.14 (0.11) mJy beam⁻¹ for a bandwidth of 240 (180) MHz. CO fluxes are measured with GILDAS. In Table 1, we list the source properties and CO measurements.

3. RESULTS

We detect CO emission in all seven targeted galaxies with integrated flux densities (I_{CO}) ranging from 0.28 to 1.18 Jy km s⁻¹. All but one have a high level of significance ($> 5\sigma$) and those resulting from ALMA observations are above the 8σ level with the exception of PACS-325 ($S/N = 4.7$). In Figure 2, we display the optical HST/ACS F814W image cutouts (Koekemoer et al. 2007) with CO and $3.6\mu m$ emission overlaid as contours. Using a large beam for the majority of the sample, the CO emission is essentially unresolved with the exception of two observations taken at higher resolution ($\sim 1''$). PACS-819 has half of the emission coming from a region of 3.2 ± 0.8 kpc, while PACS-830 is more extended (9.0 ± 1.6 kpc). This may suggest that there is diversity in the size distribution of molecular gas at high redshift (e.g., Ivison et al. 2011; Riechers et al. 2011; Hodge et al. 2012), dissimilar to local starbursts (e.g., Scoville et al. 1989).

Upon close inspection of the maps in Figure 2, it is evident that the centroid of the CO emission is not always coincident with the brightest regions of UV emission as seen in the HST/ACS image (i.e., PACS-164, PACS-830, PACS-867). This is likely evidence that a fair fraction of the star formation is obscured as supported by the improved alignment of the CO emission with the peak infrared emission detected by *Spitzer* in both the IRAC and MIPS channels, and clear association with highly significant radio emission at 1.4 GHz (Schinnerer et al. 2010).

We note that the *Herschel* far-IR (and possibly the CO) emission of PACS-164 is likely the sum of two separate components seen in the IRAC image. The peak of the CO emission, detected by IRAM, is located somewhat

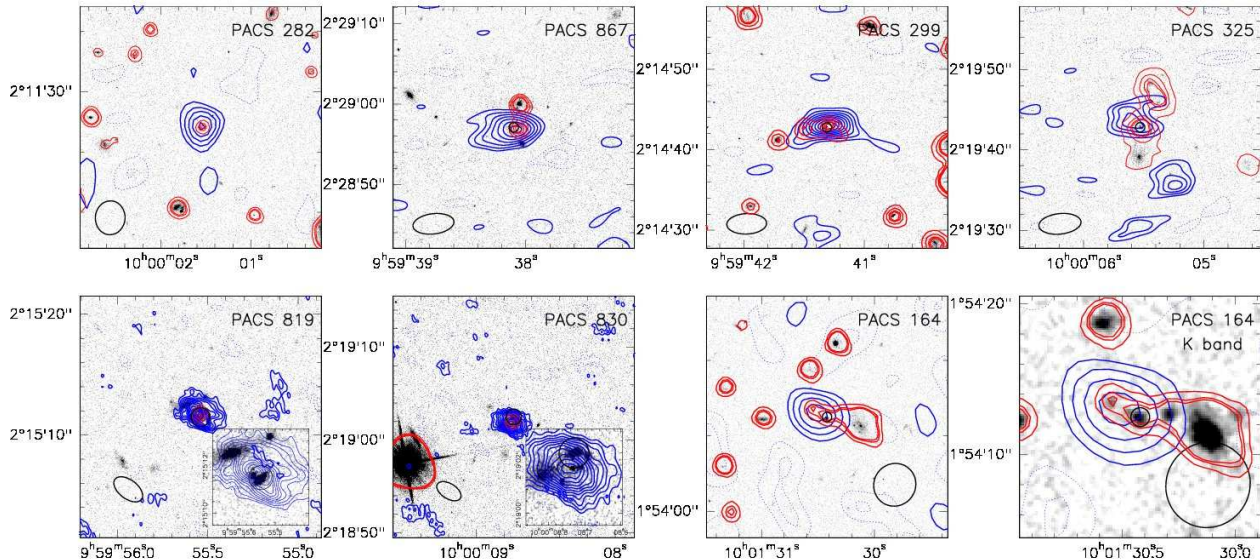


Figure 2. HST/ACS F814W images of our seven starbursts. CO emission is shown as solid (dashed) blue contours in positive (negative) steps of 1σ starting at 2 (-2) times the noise level (where σ_{rms} = 0.17, 0.12, 0.11, 0.05, 0.12, 0.14 and 0.11 mJy beam $^{-1}$ starting from left to right with 282 and then 819). *Spitzer*/IRAC 3.6 μ m detections are marked with red contours to illustrate the association of peak CO emission with their IR counterparts. CO beam size is indicated in the lower left corner. Small black circles show the placement of FMOS fibers. For PACS-164 the *K*-band image is shown to further illustrate the heavily-obscured nature of the CO-emitting region. Angular sizes of the cutouts varies.

between two IR sources, as made particularly clear by the *K*-band image also shown in Figure 2, and slightly elongated possibly indicating a contribution from both sources. The FMOS spectrum that provides the redshift ($z = 1.650$) refers to the western IR component that is co-spatial with the UV-bright source seen in the HST image. With a redshift of the CO emission ($z = 1.647$) very close to that of the FMOS source, this system appears to be in the early stages of a merger given the projected separation of 18.7 kpc. The lower limit for the stellar mass of the system as reported in Table 1 refers to the mass of the object observed with FMOS, and encircled in Figure 2.

3.1. CO-to-IR ratio

Our primary interest is to determine whether high-redshift starbursts convert gas into stars with a higher efficiency than MS galaxies at these epochs. To begin with, we use the observed CO to IR luminosity ratio L'_{CO}/L_{TIR} rather than derived quantities, e.g. the gas mass, that depends on the CO-to-H $_2$ conversion factor (α_{CO}), or gas mass surface density, which would further require CO-size information for which we only have for 2/7 galaxies in our sample. However, we note that $L'_{CO}/L_{TIR} \propto M_{gas}/SFR$ (modulo α_{CO}), hence this luminosity ratio is a fair proxy for the gas depletion time which in turn is the inverse of the SFE.

In Figure 3a, we plot L'_{CO} as a function of L_{TIR} , indicative of the obscured SFR, and include both low- and high-redshift galaxies with measurements available in the literature and compiled in Sargent et al. (2014). All line luminosities are converted to CO (1-0) using values of 0.85 and 0.7, respectively for CO (2-1) and CO (3-2) (Daddi et al. 2015). Different excitation corrections than those applied here would not impact our results since changes would either be insignificant (5 - 10% if CO (2-1) transitions were generally more excited than

assumed here) or affect only one of our sources (PACS 282, for which applying the CO(3-2)/CO(1-0) ratio of Bothwell et al. (2013) would result in a 35% difference).

All galaxies in our sample have L'_{CO}/L_{TIR} below the well-defined correlation for MS galaxies. These observations indicate the existence of an offset in the L'_{CO}/L_{TIR} ratio for high-redshift starbursts as found by Solomon et al. (1997) for local ULIRGs. In Figure 3b, we plot these quantities, normalized to the mean value of galaxies on the MS. In addition, on the abscissa we replace L_{TIR} with its implied specific SFR ($sSFR = SFR/M_*$), also normalized to the MS value. We measure a median value of $L'_{CO}/L_{CO,MS} = 0.60 \pm 0.04$ for our sample. This represents an offset $(1.7 \pm 0.1 \times)$ from the MS that is smaller than in local samples of starbursts ($\sim 3 \times$; dashed line in Fig. 3a). Along these lines, the starbursts in our sample have higher L'_{CO} than expected by ~ 0.2 dex (given their excess $sSFR$ relative to MS galaxies) based on the empirical model of Sargent et al. (2014), shown in Figure 3b.

These results may be indicative of a more continuous range in SFE, following the trend for MS galaxies (Fig. 3b) and opposed to the notion of a second mode of star-formation operating at higher efficiency distinct from MS galaxies (Daddi et al. 2010b; Genzel et al. 2010, 2015). However, any statement on differences in SFE requires a factor α_{CO} as further addressed below. Even with continuity in these parameters, there could still exist an underlying bi-modal physical framework for star formation as demonstrated with empirical models shown in Figure 3b and fully explained in Sargent et al. (2014).

3.2. Gas masses, α_{CO} , and SFE

With PACS-819 and PACS-830 having marginally resolved CO emission, we can estimate the total gas mass using the dynamical mass method (e.g., Tan et al. 2014). The dynamical mass (M_{dyn}) within the half-light radius

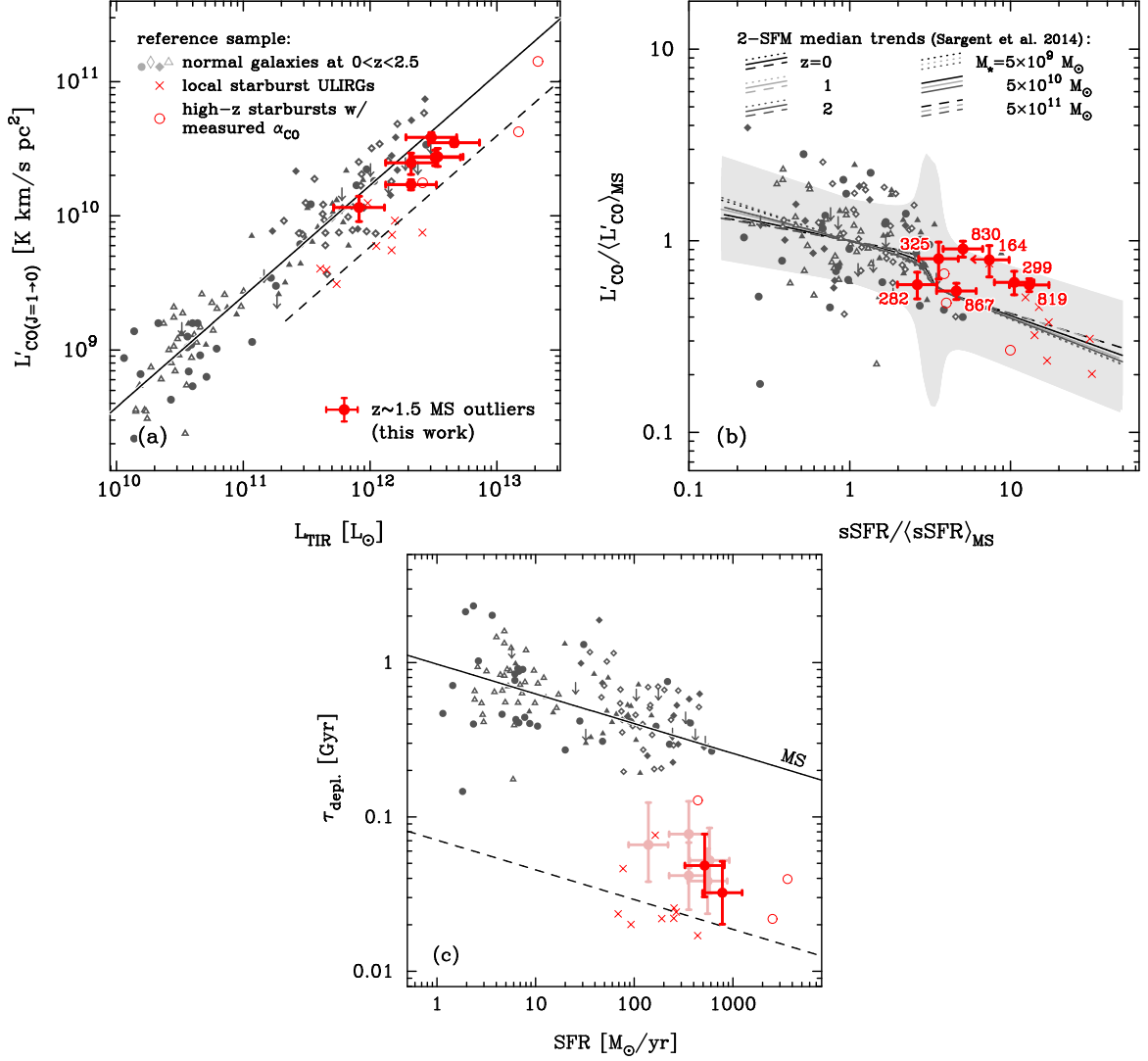


Figure 3. (a) CO luminosity versus total infrared luminosity. (b) CO luminosity and specific star formation rate with each normalized to the typical values of MS galaxies. Empirical model curves and 1σ errors (grey region) are described in Sargent et al. (2014). (c) Gas depletion time ($\tau_{\text{depl}} \equiv SFE^{-1}$; units Gyr) versus SFR. Colored symbols with error bars show our starburst sample with two (819 and 830) in bright red having dynamical mass measurements. Grey symbols represent published samples with α_{CO} estimates as compiled in Sargent et al. (2014) and shown in all panels.

($r_{1/2}$) is given for the spherically symmetric case by:

$$M_{\text{dyn}}(r < r_{1/2}) \simeq \frac{5\sigma^2 r_{1/2}}{G} \quad (1)$$

where $\sigma = \Delta v_{\text{CO}}/2.35$ is the velocity dispersion, Δv_{CO} is the line width - FWHM, and G is the gravitational constant. The gas mass is then derived by subtracting from the dynamical mass half of the stellar mass and a dark matter component ($M_{\text{DM}} = 0.25 \times M_{\text{dyn}}$; Daddi et al. 2010a) as follows.

$$M_{\text{dyn}} = 0.5 \times (M_{\star} + M_{\text{gas}}) + M_{\text{DM}}(r < r_{1/2}). \quad (2)$$

With this method, the gas mass for PACS-819 (PACS-830) is estimated to be 2.0 ± 1.2 (6.2 ± 2.2) $\times 10^{10} M_{\odot}$, based on their half-light radii, respectively 1.4 ± 0.3 kpc (4.1 ± 0.7 kpc) and velocity dispersion σ , respectively 168.0 ± 20.2 km s^{-1} (148.7 ± 20.8 km s^{-1}), that corresponds to a gas fraction $f_{\text{gas}} = M_{\text{gas}}/(M_{\text{gas}} + M_{\star})$ of 0.34 (0.46). Based on these values, we estimate

$\alpha_{\text{CO}} = 0.6 \pm 0.3$ for PACS-819 and 1.6 ± 0.6 for PACS-830, both not far from those found for the high-redshift submillimeter galaxies in the proto-cluster GN20 (Tan et al. 2014) and consistent with lower conversion factors for galaxies in mergers (Narayanan et al. 2011) as compared to isolated disk galaxies (see also Genzel et al. 2015).

We roughly estimate the H_2 gas masses from the CO line luminosity for the galaxies with unresolved CO emission using the average ($\alpha_{\text{CO}} = 1.1 M_{\odot} / \text{K km s}^{-1} \text{pc}^{-2}$) value of the two estimates of α_{CO} given above which is in very close agreement to that found for local nuclear starbursts ($\alpha_{\text{CO}} = 0.8$; Downes & Solomon 1998). Based on this conversion factor and keeping in mind the uncertainty, the gas masses are in the range $\sim (1.3 - 6.2) \times 10^{10} M_{\odot}$. This results in gas fractions $f_{\text{gas}} = M_{\text{gas}}/(M_{\text{gas}} + M_{\star})$ between 28 and 52% (see Table 1 for individual estimates), similar to those of MS galaxies at these redshifts (Tacconi et al. 2013; Béthermin et al. 2015) and in line with cosmological galaxy formation models (Narayanan et al. 2012).

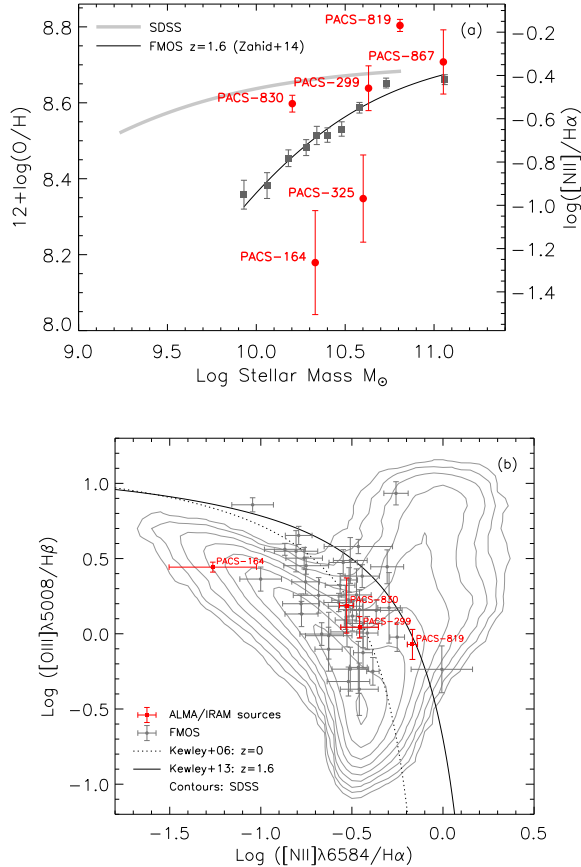


Figure 4. Rest-frame emission line ratios from FMOS-COSMOS: (a) Mass - metallicity relation of our high- z starburst sample (red points). For comparison, we plot the M-Z relation from SDSS and FMOS at $z \sim 1.6$ (Zahid et al. 2014). (b) BPT diagram at $z \sim 1.6$ (Kartaltepe et al. 2015) with our CO sample as indicated. Individual measurements, shown in grey, represent galaxies from our larger sBzK sample (Silverman et al. 2015). Contours denote the region spanned by low-redshift galaxies in SDSS. Theoretical curves separating star-forming galaxies and AGN (that evolve with redshift) are given. All data points have $\pm 1\sigma$ errors.

Based on these results, an increase in the SFE is likely responsible for their elevation above the MS. In Figure 3c, we illustrate this scenario by plotting the gas depletion timescale ($\tau_{\text{del}} \equiv \text{SFE}^{-1}$; units Gyr) as a function of SFR. As described above, the lower CO luminosities at a given L_{TIR} , compared to MS galaxies, are indicative of a lower gas mass hence shorter gas depletion timescales and higher SFEs, in agreement with previous studies (Genzel et al. 2010; Daddi et al. 2010b). Despite the remaining uncertainties on the assumptions used to derive H_2 masses, we see evidence that starbursts in our sample have a smaller contrast (i.e., less extreme) in SFE, relative to MS galaxies, as compared to local ULIRGs and the strongest starbursts at high- z .

As a final check, we can assess whether the values of α_{CO} derived above are appropriate for our starbursts by using the metallicity of the ISM as a proxy, given that it is well established that α_{CO} is anti-correlated with metallicity (e.g., Arimoto, Sofue & Tsujimoto 1996; Schrubba et al. 2012; Genzel et al. 2012). In Figure 4a, we show the mass-metallicity relation at $z \sim 1.6$ (Zahid et al. 2014) based on $[\text{NII}]\lambda 6585/\text{H}\alpha$, with our

sample shown in red. We find that 4 out of 6 galaxies (having errors $< \pm 0.2$ on the ratio) have high metallicities, similar to those of local massive galaxies. Therefore, our derived values of α_{CO} are consistent with local galaxies of a similar mass and metallicity, although with the caveat that we are not certain whether the metallicity of the line-emitting gas is representative of the molecular gas producing the CO emission.

We also examine whether AGN photo-ionization is contributing to the high $[\text{NII}]/\text{H}\alpha$ ratios seen in some of our galaxies. Figure 4b shows the FMOS-COSMOS version of the BPT diagram at $z \sim 1.6$. Four galaxies with CO measurements have all key diagnostic lines detected by FMOS. None of our galaxies fall in the region where strong AGN contribution is expected, above the line separating AGN from star-forming galaxies at $z \sim 1.6$ (Kewley et al. 2013). While PACS-819 approaches this line, it is not detected in X-rays with *Chandra*. Nevertheless, we cannot rule out the presence of a low-to-moderate luminosity AGN, especially because its strong $[\text{NII}]$ emission also drives this galaxy above the local MZ relation. For reference, in Figure 4b, we plot the data for the larger star-forming galaxy population from FMOS-COSMOS (grey data points). It is worth highlighting that both PACS-830 and PACS-299 fall within the locus of the star-forming population, clearly offset towards a higher ionization state of the ISM compared to local galaxies (Steidel et al. 2014; Kartaltepe et al. 2015).

4. CONCLUDING REMARKS

Our observations of the molecular CO gas content of seven galaxies well-above the MS at $z \sim 1.6$ with ALMA in Cycle 1 and IRAM/PdBI establish an offset in the $L'_{\text{CO}} - L_{\text{TIR}}$ relation for starbursts at high redshift, compared to MS galaxies, although smaller than expected from previous studies of low- z starburst outliers. These results may be indicative of a continuous distribution in SFE at high redshift, as a function of distance from the star-forming MS, as opposed to a bi-modal distribution.

An appealing physical explanation for a decrease in the $L'_{\text{CO}}/L_{\text{TIR}}$ ratio for galaxies well-above the MS is galaxy mergers that can lead to rapid gas compression hence effectively boosting star formation resulting in shorter gas depletion timescales. Several galaxies well-above the MS are indeed in a merger phase (Rodighiero et al. 2011; Wuyts et al. 2011). Within the present sample, hints of merging come from the presence of multiple UV/optical emitting regions (e.g., in PACS-819, PACS-830, PACS-867), even being in a kinematically-linked system (PACS-164).

We are grateful for the support from the regional ALMA ARCs, in particular Akiko Kawamura, Kazuya Saigo, Gaelle Dumas and Sergio Martin. JDS was supported by the ALMA Japan Research Grant of NAOJ Chile Observatory, NAOJ-ALMA-0127. This work was supported by World Premier International Research Center Initiative (WPI Initiative), MEXT, Japan. CM and AR acknowledge support from an INAF PRIN 2012 grant. This paper makes use of the following ALMA data: ADS/JAO.ALMA#2012.1.00952.S. ALMA is a partnership of ESO (representing its member states), NSF (USA) and NINS (Japan), together with NRC

(Canada), NSC and ASIAA (Taiwan), and KASI (Republic of Korea), in cooperation with the Republic of Chile. The Joint ALMA Observatory is operated by ESO, AUI/NRAO and NAOJ.

REFERENCES

- Arimoto, N., Sofue, Y., Tsujimoto, T. 1996, PASJ, 48, 275
 Béthermin, M., Daddi, E., Magdis, G., et al. 2015, A&A, 573, A113
 Bothwell, M.S., Smail, I., Chapman, S.C. et al. 2013, MNRAS, 429, 3047
 Bouché, N., Dekel, A., Genzel, R., et al. 2010, ApJ, 718, 1001
 Bruzual, G., & Charlot, S. 2003, MNRAS, 344, 1000
 Casey, C. M., Chapman, S. C., Neri, R. et al. 2011, MNRAS, 415, 2723
 Daddi, E., Dickinson, M., Morrison, G. et al. 2007, ApJ, 670, 156
 Daddi, E., Bournaud, F., Walter, F. et al. 2010a, ApJ, 713, 686
 Daddi, E., Elbaz, D., Walter, F. et al. 2010b, ApJ, 714, L118
 Downes, D., & Solomon, P. M. 1998, ApJ, 507, 615
 Draine, B. T., Li, A. 2007, ApJ, 657, 810
 Elbaz, D., Daddi, E., Le Borgne, D. et al. 2007, A&A, 468, 33
 Genzel, R., Tacconi, L. J., Gracia-Carpio, J., et al. 2010, MNRAS, 407, 2091
 Genzel, R., Tacconi, L. J., Combes, F., et al. 2012, ApJ, 746, 69
 Genzel, R., Tacconi, L. J., Lutz, D., et al. 2015, ApJ, 800, 20
 Greve, T. R., Bertoldi, F., Smail, I. et al. 2005, MNRAS, 359, 1165
 Hodge, J. A., Carilli, C. L., Walter, F. et al. 2012, ApJ, 760, 11
 Ilbert, O., Arnouts, S., Le Floc'h et al. 2015, A&A, 579, 2
 Ivison, R. J., Papadopoulos, P. P., Smail, I. et al. 2011, MNRAS, 412, 1913
 Kartaltepe, J. Sanders, D. B., Silverman, J. D. et al., ApJ, 806, L35
 Kashino, D., Silverman, J., Rodighiero, G. et al. ApJ, 777, L8
 Kewley, L., Dopita, M., Leitherer, C., et al. 2013, ApJ, 774, 100
 Koekemoer, A. et al. 2007, ApJS, 172, 196
 Lilly, S. J., Carollo, C. M., Pipino, A., 2013, ApJ, 772, 119
 Lilly, S. J., Le Fèvre, O., Renzini, A., et al. 2013, ApJS, 772, 119
 Madau, P., & Dickinson, M. 2014, ARA&A, 52, 415
 Magdis, G. E., Daddi, E., Béthermin, M. 2012, ApJ, 760, 6
 Magnelli, B., Lutz, D., Saintonge, A. et al. 2014, A&A, 561, 86
 Narayanan, D., Krumholz, M., Ostriker, E. C., & Hernquist, L. 2011, MNRAS, 418, 664
 Narayanan, D., Bothwell, M., & Davé, R. 2012, MNRAS, 426, 1178
 Noeske, K., Weiner, B. J., Faber, S. M. et al. 2007, ApJ, 660, L43
 Pozzi, F., Vignali, C., Gruppioni, C. et al. 2012, MNRAS, 423, 1909
 Riechers, D. A., Hodge, J., Walter, F., Carilli, C. L., Bertoldi, F. 2011, ApJ, 739
 Rodighiero, G., Daddi, E., Baronchelli, I. et al. 2011, ApJ, 739, L40
 Sanders, D. B. & Mirabel, I. F. 1996, ARA&A, 34, 749
 Santini, P., Maiolino, R., Magnelli, B. 2014, A&A, 562, A30
 Sargent, M. T., Daddi, E., Béthermin, M. et al. 2014, ApJ, 793, 19
 Schinnerer, E., Sargent, M. T., Bondi, M. et al. 2010, ApJS, 188, 384
 Schrubba, A., Leroy, A. K., Walter, F. et al. 2012, AJ, 143, 138
 Scoville, N. Z., Sanders, D. B., Sargent, A. I. et al. 1989, ApJ, 345, L25
 Scoville, N. Z., Aussel, H., Sheth, K. et al. 2014, ApJ, 783, 84
 Silverman, J. D., Kashino, D., Arimoto, N. et al. 2015, ApJS, 220, 12
 Solomon, P. M., Downes, D., Radford, S. J. E., & Barrett, J. W. 1997, ApJ, 478, 144
 Speagle, J. S., Steinhardt, C. L., Capak, P. L., Silverman, J. D. 2014, ApJS, 214, 15
 Steidel, C. C., Rudie, G. C., Strom, A. L. et al. 2014, ApJ, 795, 165
 Swinbank, A. M., Simpson, J. M., Smail, I. et al. 2014, MNRAS, 438, 1267
 Tacconi, L., Genzel, R., Neri, R., et al. 2010, Nature, 463, 781
 Tacconi, L., Neri, R., Genzel, R., et al. 2013, ApJ, 768, 74
 Tan, Q., Daddi, E., Magdis, G. et al. 2014, A&A, 569, A98
 Whitaker, K. E., van Dokkum, P. G., Brammer, G. et al. 2012, ApJ, 754, L29
 Wuyts, S., Förster Schreiber, N. M., van der Wel, A. et al. 2011, ApJ, 742, 96
 Zahid, H. J., Kashino, D., Silverman, J. D., et al. 2014, ApJ, 792, 75